Journal of
Materials Chemistry A

Materials for energy and sustainability

ROYAL SOCIETY
OF CHEMISTRY
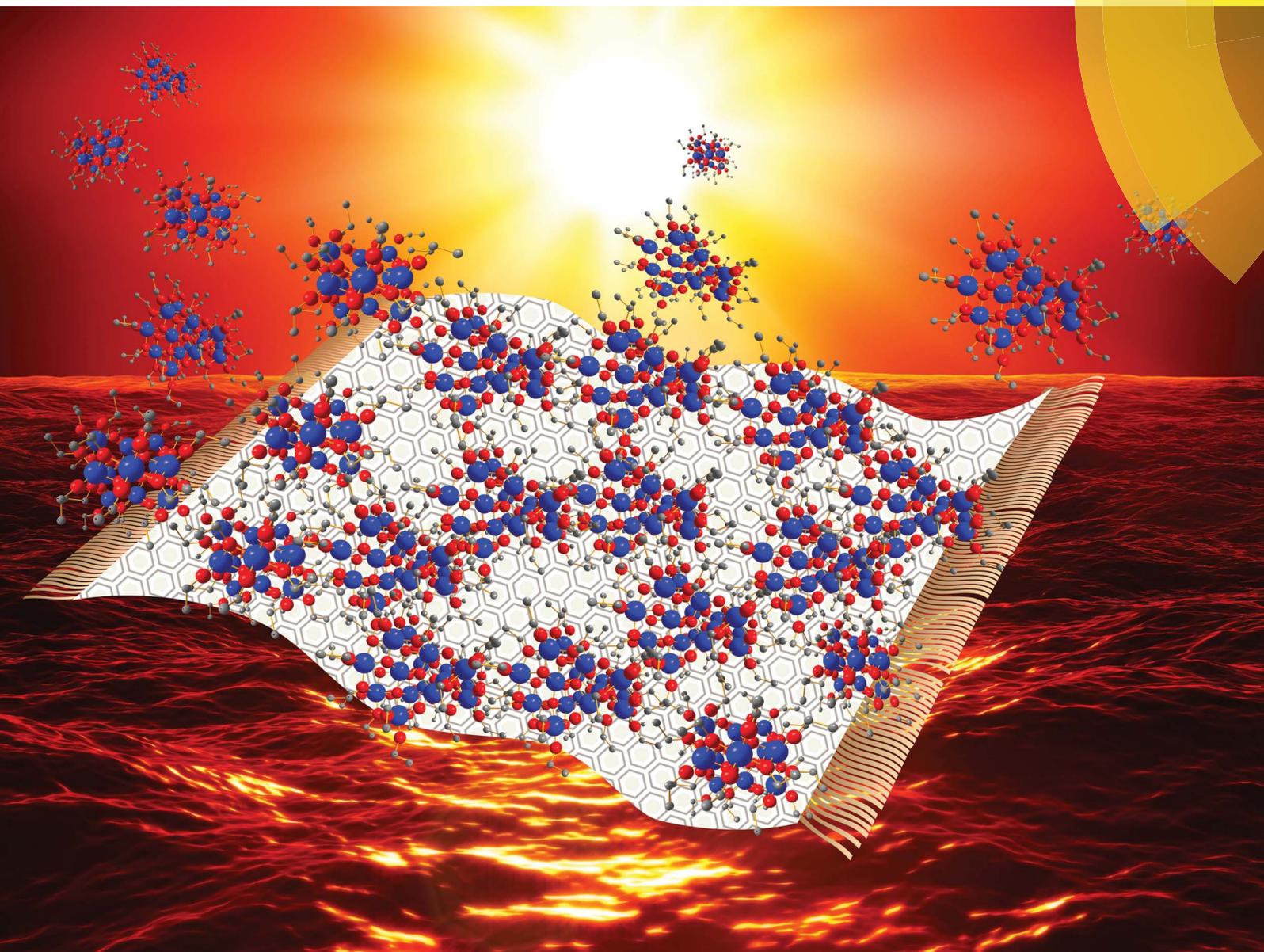
PAPER
Salvador Eslava *et al.*
Using graphene oxide as a sacrificial support of polyoxotitanium clusters
to replicate its two-dimensionality on pure titania photocatalysts

175 YEARS

PAPER

Using graphene oxide as a sacrificial support of polyoxotitanium clusters to replicate its two-dimensionality on pure titania photocatalysts†

Salvador Eslava,*[a] Anna Reynal,[b] Victoria G. Rocha,[c] Suelen Barg[d] and Eduardo Saiz[c]

The nanostructure optimisation of metal oxides is of crucial importance to exploit their qualities in artificial photosynthesis, photovoltaics and heterogeneous catalysis. Therefore, it is necessary to find viable and simple fabrication methods to tune their nanostructure. Here we reveal that graphene oxide flakes, known for their nano- and two-dimensionality, can be used as a sacrificial support to replicate their nano- and two-dimensionality in photocatalytic titania. This is demonstrated in the calcination of $Ti_{16}O_{16}(OEt)_{32}$ polyoxotitanium clusters together with graphene oxide flakes, which results in pure titania nanoflakes of <10 nm titania nanoparticles in a two-dimensional arrangement. These titania nanoflakes outperform the titania prepared from only $Ti_{16}O_{16}(OEt)_{32}$ clusters by a factor of forty in the photocatalytic hydrogen production from aqueous methanol suspensions, as well as the benchmark P25 titania by a factor of five. These outcomes reveal the advantage of using polyoxotitanium clusters with graphene oxide and open a new avenue for the exploitation of the vast variety of polyoxometalate clusters as precursors in catalysis and photovoltaics, as well as the use of graphene oxide as a sacrificial support for nanostructure optimisation.

Introduction

By 2050, it is expected that the world energy demand will double, due to the growth in human population and the development of heavily populated countries such as China and India.[1,2] In parallel, fossil fuel resources are dwindling, becoming more expensive and contributing to the increase in carbon dioxide (CO_2) emissions which exacerbate global warming. Artificial photosynthesis offers an opportunity to exploit inexhaustible solar energy. UV and visible light absorbing semiconductor photocatalysts such as TiO_2, ZnO, CdS, Fe_2O_3, WO_3, Cu_2O and various combinations forming heterojunctions have proved to photocatalytically generate solar fuels from water and/or carbon dioxide.[3–9] However, further research and progress is necessary to increase the current low yields of product formation. The low efficiency of these photocatalytic systems has commonly been attributed to the lack of absorption of visible light, low surface area, fast recombination of photogenerated charge carriers and back reactions of reduced species to form CO_2 and/or H_2O. To make artificial photosynthesis economically viable, significant improvements in the properties of the photocatalysts are needed. Here we focus on improving the nanostructure of titania photocatalysts, i.e. the morphology and surface area, for more effective light exposure and dispersion in aqueous systems.

Polyoxotitanium clusters, also called cages, of the type $Ti_xO_y(OR)_z$ (OR = alkoxide) are currently receiving much attention for their use as well-defined precursors in the formation of metal oxides with great potential in photovoltaics and catalysis.[10–24] Novel synthetic routes have extended the family and achieved a wide variety of heterometallic oxo clusters containing Fe, Cu, Co, and Ni of the type $Ti_xO_y(OR)_zM_mX_n$ (OR = alkoxide; M = main group transition metal or lanthanide; X = anion such as a halide).[16–18] Exploiting the full potential of these polyoxometalate clusters as precursors for the preparation of highly crystalline nanostructured metal oxides requires finding simple methods or strategies to achieve their full oxidation and crystallisation while obtaining the desired morphology and texture for the final application.

Graphene oxide (GO) is a flat monolayer of carbon atoms bearing oxygen-containing functional groups and having a unique nano- and two-dimensionality.[25] Unlike graphene, GO can be dispersed in different solvents due to its functional organic groups (epoxides, hydroxyls and carboxylic groups), which permit its utilisation in wet chemical processes.[26] It is typically used as a precursor to reduced graphene oxide (RGO), a chemically derived graphene,[26] which has been used in the

[a]Department of Chemical Engineering, University of Bath, Bath BA2 7AY, UK. E-mail: s.eslava@bath.ac.uk

[b]School of Science and Engineering, Teesside University, Middlesbrough TS1 3BA, UK

[c]Centre for Advanced Structural Ceramics, Department of Materials, Imperial College London, London SW7 2BP, UK

[d]School of Materials, University of Manchester, Oxford Rd, Manchester M13 9PL, UK

† Electronic supplementary information (ESI) available: Histogram of GO flakes and Raman characterisation. See DOI: 10.1039/c5ta09989g

7200 | J. Mater. Chem. A, 2016, 4, 7200–7206

This journal is © The Royal Society of Chemistry 2016

formation of heterojunctions with photocatalysts to minimise electron–hole recombination by electron transfer between the photocatalyst and the RGO.[27–33] However, the formation of high quality heterojunctions with oxide photocatalysts is hampered by a trade-off between the photocatalyst and the RGO formation: on one hand, the photocatalyst precursors need to be annealed in an oxidising atmosphere for complete oxidation and crystallisation, and on the other hand, the GO needs to be annealed in a reducing atmosphere to restore the sp^2 bonding structure and to be conductive. For this reason, most RGO-photocatalyst heterojunctions are typically prepared by solvothermal treatment at temperatures not higher than 200 °C. This trade-off compromises the enhancement of the photocatalytic performance with respect to the single photocatalyst and the utilisation of RGO in the devices' fabrication.

In this paper, we reveal another use of graphene oxide, as a sacrificial support, and demonstrate that this facilitates exploiting the polyoxometalate cluster $Ti_{16}O_{16}(OEt)_{32}$ as the precursor for the formation of titania with a unique optimised nanostructure. We show that the formed titania, despite not containing GO in its final version, replicates the GO shape, being arranged in a two-dimensional arrangement as nanoflakes. These titania nanoflakes clearly outperform the benchmark P25 titania by a factor of five in solar hydrogen generation with methanol as a hole scavenger. This strategy offers new ways to exploit both the plethora of polyoxometalate clusters as precursors for solar-to-fuels photocatalysts and graphene oxide's two-dimensionality as a unique sacrificial support.

Experimental

All manipulations were done in air but vessels were kept closed when possible. Chemicals for the synthetic part of this work were purchased from commercial suppliers and used without further purification.

$Ti_{16}O_{16}(OEt)_{32}$ clusters were prepared by a well-established synthesis method, as reported previously.[34] Briefly, 14 mL of $Ti(OEt)_4$ (Alfa Aesar, 99+%), 14 mL of anhydrous ethanol (Sigma Aldrich) and 600 μL of doubly deionised water were placed in a 45 mL Teflon-lined stainless steel autoclave and heated to 100 °C for 14 days. Slow cooling to room temperature gave mm- and cm-size colourless crystals of $Ti_{16}O_{16}(OEt)_{32}$ clusters (~60% yield). Elemental analysis (wt%) calculated for $C_{64}H_{160}O_{48}Ti_{16}$: C 31.2, H 6.5; found: C 31.3, H 6.5.

Graphene oxide (GO) was prepared by oxidation and exfoliation of graphite, using a modified Hummer's method.[35] Briefly, 10 g of 100–500 μm graphite particles (Sigma Aldrich) was oxidised in a mixture of 620 g of 95% sulfuric acid, 7.5 g of sodium nitrate and 45 g of potassium permanganate under vigorous overhead stirring. Overheating was avoided with a cooling jacket at 10 °C. After 3 h reaction, 40 mL of doubly deionised water was added and the mixture was kept at room temperature under vigorous stirring for 3 days. Next, 1 L of doubly deionised water and 30 g of aqueous hydrogen peroxide (30% wt) were slowly added to stop the reaction. The GO was then washed by diluting, centrifuging and redispersing in doubly deionised

water at least ten times. Finally, the GO was freeze-dried for storage. Elemental analysis (wt%) found: C 42.6, H 0.9, N 1.0.

Two types of titania particles were prepared. For the preparation of the first type, 1 g of $Ti_{16}O_{16}(OEt)_{32}$ clusters was dissolved in 10 mL of anhydrous tetrahydrofuran (THF). 0.031 g of GO (3% of final solid weight) was dispersed in 10 mL of THF by alternating sonication and stirring for 3 h. Both samples were mixed dropwise under vigorous stirring, and kept under stirring for 10 min. The solvent was then evaporated under stirring in an oil bath at 70 °C. The mixture was further dried in an oven at 70 °C overnight. Finally, the dried mixture was heated with a ramp rate of 10 °C min^{-1} to 450 °C and kept at this temperature for 1 h. It should be noted that at this temperature, most of the GO is sacrificed and $Ti_{16}O_{16}(OEt)_{32}$ clusters are oxidised to titania (TiO_2). The same procedure for dissolving the $Ti_{16}O_{16}(OEt)_{32}$ clusters, drying and calcining was followed to prepare a second titania sample, but this time without the addition of the GO. No co-catalysts, e.g. Pt, were used in the syntheses or photocatalytic tests.

Photocatalytic tests

100 mg of calcined titania particles was placed in a 180 mL quartz reaction vessel with a mixture of 20 mL of methanol and 80 mL of distilled water. The suspension was first sonicated for 30 min and then kept under stirring for the remainder of the experiment. The liquid and headspace were purged with argon for 30 min with a gas flow of approx. 100 mL min^{-1} to remove oxygen. Next, the argon flow passing through the reactor was lowered to 5 mL min^{-1} and directly connected to a gas chromatograph (GC, Perkin Elmer Clarus 580GC) for monitoring the gas evolution in the reactor with a 1 μL gas sampling valve automated system. The GC used helium as a carrier gas, a 5 Å molecular sieve column and a discharge ionisation detector (DID). The photocatalytic reaction was carried out by laterally irradiating the suspension with a solar simulator for 3 h. The irradiation source consisted of a 75 W Xe lamp (Hamamatsu RC0020). In order to simulate the solar spectrum, an AM 1.5G filter and neutral density filters were used, adjusting the intensity to 100 mW cm^{-2} at the position of the quartz reaction vessel.

Characterisation

Elemental analysis was carried out on a Thermo Scientific Flash 2000 configured for %CHN. Images were obtained by field emission gun scanning electron microscopy (FEG-SEM) LEO1525 with an acceleration voltage of 5 kV and by transmission electron microscopy (JEOL JEM1200EXII). For better contrast in SEM, titania particles were deposited on highly doped n^{++}-type Si wafer and GO on 300 nm SiO_2 coated n-type Si wafer. Powder X-ray diffraction (XRD) patterns in the 2 theta range 10–70° were measured on a Bruker D2 PHASER desktop diffractometer using Cu-K$_\alpha$ radiation, with a total integration time of 1232 s. Nitrogen adsorption at 77 K was carried out using an Autosorb-6B (Quanta Chrome). Samples were first degassed in an Autosorb degasser (Quanta Chrome) under 0.03 mbar for at least 24 h before nitrogen adsorption. Surface areas were calculated using the Brunauer–Emmett–Teller (BET)

method. The equivalent-spherical particle size distributions in suspension after the photocatalytic tests were measured by laser beam scattering technique using a Malvern Mastersizer 2000 particle size analyser. The ζ-potential of particles in aqueous methanol suspensions was measured by a Malvern Zetasizer Nano ZS.

Results and discussion

$Ti_{16}O_{16}(OEt)_{32}$ clusters were prepared by well-established solvothermal synthesis using $Ti(OEt)_4$, ethanol and a controlled amount of water. Resulting clusters were isolated by crystallisation in mm- and cm-size crystals. CHN elemental analysis confirms the formation of $Ti_{16}O_{16}(OEt)_{32}$ (wt% calculated for $C_{64}H_{160}O_{48}Ti_{16}$: C 31.2, H 6.5; found: C 31.3, H 6.5). Fig. 1a shows its compact structure, which exhibits four μ_4-oxo, eight μ_3-oxo, four μ_2-oxo and sixteen μ_2-OEt bridging ligands and sixteen OEt terminating ligands connected to sixteen octahedral titanium atoms. Two orthogonal blocks of eight TiO_6 octahedra compose the titanium oxo core $[Ti_{16}O_{16}]$. The GO was prepared by oxidation and exfoliation of graphite. Fig. 1b shows SEM images of GO spread on SiO_2/Si wafer. The GO flakes have a wide size distribution, with most abundant maximum lateral sizes being between 2 and 4 μm. A histogram with the flake size distribution is shown in ESI (Fig. S1†).

Two types of titania particles were prepared by dissolving $Ti_{16}O_{16}(OEt)_{32}$ clusters in THF solvent with or without the addition of GO, drying and then calcining at 450 °C. These conditions were used to ensure the sacrifice of the GO and the oxidation of $Ti_{16}O_{16}(OEt)_{32}$ clusters to titania (TiO_2). The photocatalytic hydrogen production of these titania particles was tested in 20% vol. aqueous methanol solution while irradiating with a solar simulator. Fig. 2 shows the hydrogen production rate *vs.* time measured at the outlet of the photocatalytic reactor and Table 1 shows the averaged hydrogen production rate. The titania prepared from only $Ti_{16}O_{16}(OEt)_{32}$ clusters produces 5.5 μmol H_2 g^{-1} h^{-1}. The photocatalytic response of the benchmark P25 titania was also tested in the same conditions for comparison. P25 titania produces 42.8 μmol H_2 g^{-1} h^{-1}, showing that the titania prepared by dissolving, drying and

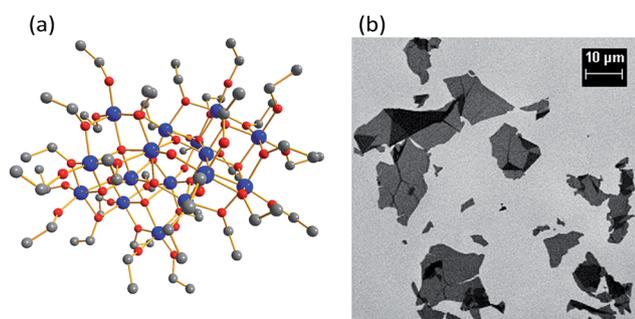Fig. 1 (a) Structure of the $Ti_{16}O_{16}(OEt)_{32}$ cluster. Titanium, oxygen and carbon atoms are represented by blue, red and grey balls, respectively. Hydrogen atoms and the minor components of disorder in some of the EtO groups are omitted for clarity. (b) SEM image of GO spread on SiO_2/Si wafer.
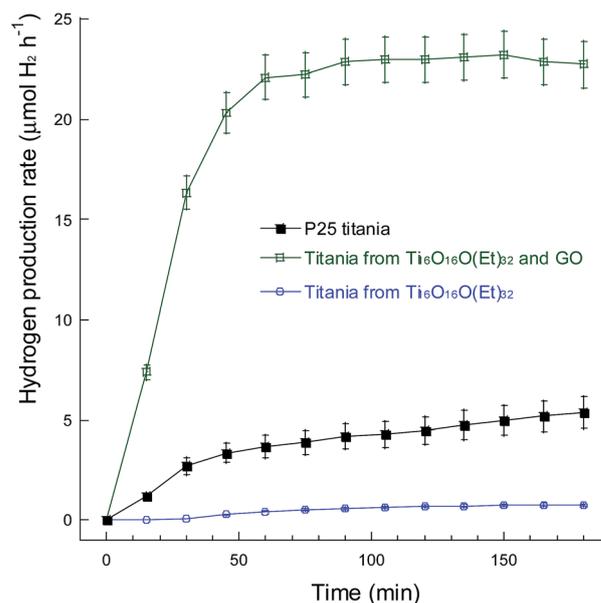

Fig. 2 Hydrogen production rates measured at the outlet stream of a photocatalytic reactor irradiated with a solar simulator and containing 20 mL of methanol, 80 mL of distilled water and 100 mg of titania. Titania powders were prepared by dissolving, drying and calcining $Ti_{16}O_{16}(OEt)_{32}$ clusters, with or without GO. The results for P25 titania are included for reference. The reactor is continuously purged with argon and the hydrogen rate is measured at the outlet.

calcining at 450 °C $Ti_{16}O_{16}(OEt)_{32}$ clusters is of inferior performance. We reveal, however, that dissolving, drying and calcining $Ti_{16}O_{16}(OEt)_{32}$ clusters leads to a titania far superior to P25 titania if clusters are supported on GO before drying and calcining. Fig. 2 shows that the titania following this approach produces 223.8 μmol H_2 g^{-1} h^{-1}, five times more than P25 titania and forty times more than titania prepared from only $Ti_{16}O_{16}(OEt)_{32}$ clusters (Table 1). Thus, the combination of $Ti_{16}O_{16}(OEt)_{32}$ clusters and GO for the synthesis of titania appears to be crucial. Further experiments were performed in order to shed some light on these outcomes.

SEM and TEM images of the different titania particles are shown in Fig. 3. The titania prepared from only $Ti_{16}O_{16}(OEt)_{32}$ clusters has a particle size in the micrometre range, with large particles with a diameter >5 μm (Fig. 3a). TEM shows that these μm size particles consist of globular aggregates of 12 ± 3 nm nanoparticles (Fig. 3b). When the GO is used with $Ti_{16}O_{16}(OEt)_{32}$ clusters, the diameter of the final titania particles decreases to 8 ± 3 nm and they are mostly arranged as flakes similar in shape to the original GO flakes (Fig. 3c–e). These titania nanoparticles are 3 times smaller than P25 titania particles, which are 20–35 nm in diameter (Fig. 3f and g). The smaller particle size and consequently higher surface area is in line with the higher photocatalytic hydrogen production rate (Fig. 2). Moreover, their arrangement in two-dimensional flakes can help to minimise the light shielding and therefore improve the photocatalytic performance. Practically no GO is found on the SEM or TEM inspection of this titania (only very few fragments were observed), so in the current calcination conditions, the GO must have completely

7202 | J. Mater. Chem. A, 2016, 4, 7200–7206

This journal is © The Royal Society of Chemistry 2016

Table 1 Measured properties of prepared titania powders and P25 titania, for comparison

Sample	H_2 production ($\mu mol\ g^{-1}\ h^{-1}$)	BET surface area ($m^2\ g^{-1}$)	Carbon content (% wt)	ζ-Potential (mV)
Titania from $Ti_{16}O_{16}(OEt)_{32}$	5.5 ($\pm$0.6)	24 ($\pm$2)	1.3 ($\pm$0.1)	−29.0 ($\pm$1.5)
Titania from $Ti_{16}O_{16}(OEt)_{32}$–GO	223.8 ($\pm$11)	62 ($\pm$3)	0.61 ($\pm$0.03)	0.7 ($\pm$8.3)
P25 titania	42.8 ($\pm$6)	55 ($\pm$3)	<0.1	−0.3 ($\pm$1.0)

gasified to oxidised species such as CO_2 and CO. The absence of graphene derivatives in the prepared titania is further confirmed by Raman spectroscopy (Fig. S2 in ESI†).

The crystalline phase of the prepared titania powders is pure anatase, unlike P25 titania, which is approx. 80% anatase and 20% rutile (Fig. 4). Table 1 shows the carbon content, measured by elemental analysis. Unlike P25 titania, which is known to be prepared in an oxy-hydrogen flame (temperatures up to ~2000 °C),[36] occluded carbon is expected in these titania powders prepared at 450 °C. The titania prepared from only $Ti_{16}O_{16}(OEt)_{32}$ clusters contains 1.3 ± 0.1% wt occluded carbon. The addition of the GO to the synthesis procedure lowers the carbon content to 0.61 ± 0.03% wt. This indicates that supporting the $Ti_{16}O_{16}(OEt)_{32}$ clusters on GO, known for being two-dimensional and with a high surface area,[37,38] substantially facilitates the air exposure of titania precursors and therefore their oxidation and/or conversion to titania (TiO_2) during the calcination.

The titania powders were characterised by N_2 adsorption (Fig. 5) and their surface area was calculated using the BET method and reported in Table 1. The lowest surface area is reported for the titania prepared from $Ti_{16}O_{16}(OEt)_{32}$ clusters, 24 $m^2\ g^{-1}$, in agreement with its relatively poor performance in the photocatalytic hydrogen production. The addition of the GO to the synthesis procedure increases the final powder surface area, which more than doubles to 62 $m^2\ g^{-1}$. For comparison, P25 titania has a surface area of 55 $m^2\ g^{-1}$. Comparison of the surface areas with the hydrogen production indicates that the higher the surface area, the higher the photocatalytic hydrogen production. However, the relation is not linear, so other factors such as nanoparticle size and aggregate shape & size also influence the final performance.

Together with the surface area and particle size, the shape and size of particle agglomerates in the reacting suspensions are also critical in determining the photocatalytic activity because they strongly affect the suspension of the particles as well as their light scattering and absorption. Titania powders prepared from only $Ti_{16}O_{16}(OEt)_{32}$ were coarse and difficult to disperse in water and methanol, despite sonication and stirring. However, the titania powders prepared from $Ti_{16}O_{16}(OEt)_{32}$ and GO dispersed very easily in water and methanol, similarly to P25 titania. Laser beam scattering analysis was carried out to provide insights into the dispersion of these particles in water. The size range of analysis for laser beam scattering is typically above 0.2 μm for equivalent-spherical particles. The number-weighted equivalent-spherical particle size distributions show that the titania prepared from $Ti_{16}O_{16}(OEt)_{32}$ clusters, with or without GO, reaches smaller particle or agglomerate sizes in

suspension compared to P25 titania, with a monomodal distribution with a maximum at 0.36 μm compared to a bimodal distribution with maxima at 0.41 and 2.2 μm for P25 titania (Fig. 6a). Unlike a number-weighted distribution where each particle is given equal weighting irrespective of its size, in a volume-weighted distribution, the intensity is proportional to (radius),[3] so larger particles hold higher weight than smaller particles in the distribution.[39] Fig. 6b shows the volume-weighted equivalent-spherical particle or agglomerate size distributions in suspension. All types of titania, including P25, contain agglomerates or particles in the micrometre range, with their main size distribution centred between 5 and 50 μm. P25 titania nanoparticles are aggregated to agglomerates with a broad size distribution centred at 6 μm. The titania prepared from $Ti_{16}O_{16}(OEt)_{32}$ clusters contains particles or agglomerates with a wide distribution centred at 15 μm and smaller particles or agglomerates down to 0.25 μm. When GO is added to the synthesis procedure, the distribution maximum of the resulting titania particles or agglomerates decreases from 15 to 5 μm, while keeping particles down to 0.25 μm. A few agglomerates are present above 100 μm and the addition of GO to the synthesis procedure does not seem to affect them. In summary, the laser beam scattering confirms the benefits of adding GO to the formation of photocatalytic titania, leading to a titania easier to disperse and irradiate in aqueous suspensions because of finer particle or agglomerate size.

The ζ-potential, or electrokinetic potential, is related to the colloidal properties of particle suspensions and the particle size. Suttiponparnit et al. demonstrated in a set of titania samples with different particle sizes that the ζ-potential becomes more positive for smaller particles at any pH.[40] The titania prepared from $Ti_{16}O_{16}(OEt)_{32}$ clusters in 20% vol. aqueous methanol suspensions (neutral pH) have a ζ-potential around −30 mV, which becomes more positive when GO is used in the synthesis (Table 1). In the case of titania prepared from $Ti_{16}O_{16}(OEt)_{32}$ together with GO, the ζ-potential is around 0 mV, like that of P25 titania. This demonstrates another clear effect of GO as a sacrificial support on the final colloidal properties of the resulting titania and in decreasing the particle size.

SEM images, Raman spectroscopy and XRD show no signs of GO or its reduced version (reduced GO, RGO) in the final titania. In photocatalytic composites or hybrids published in literature involving GO, the GO is typically reduced to RGO by solvothermal treatment to temperatures around 200 °C.[27–33] Wrinkled flakes are easily observed by SEM in these composites or hybrids, and Raman signals are assigned to C sp^2. RGO is not completely transparent, so it compromises the light irradiation
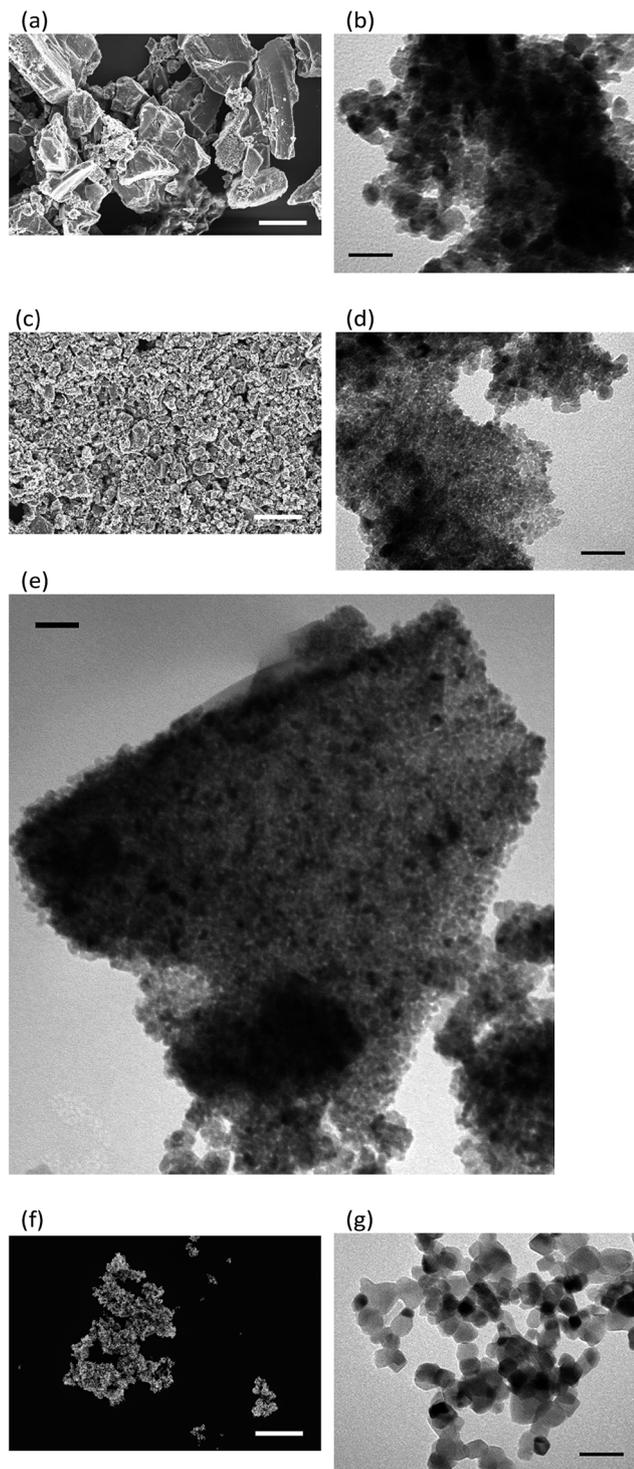
This journal is © The Royal Society of Chemistry 2016

J. Mater. Chem. A, 2016, 4, 7200–7206 | 7203

Fig. 3 SEM and TEM images of titania particles prepared by dissolving, drying and calcining (a and b) $Ti_{16}O_{16}(OEt)_{32}$ clusters and (c–e) $Ti_{16}O_{16}(OEt)_{32}$ clusters and GO. (f and g) SEM and TEM images of P25 titania, for comparison. Scale bar in all SEM images (a, c, f): 5 μm. Scale bar in all TEM images (b, d, e, g): 50 nm.

of the photocatalyst composites or hybrids, but it is reported that by using limited amounts of RGO (<3% wt), the shielding effect is overcome by minimised electron–hole recombination.[27] In this work, the synthesis conditions (with temperatures
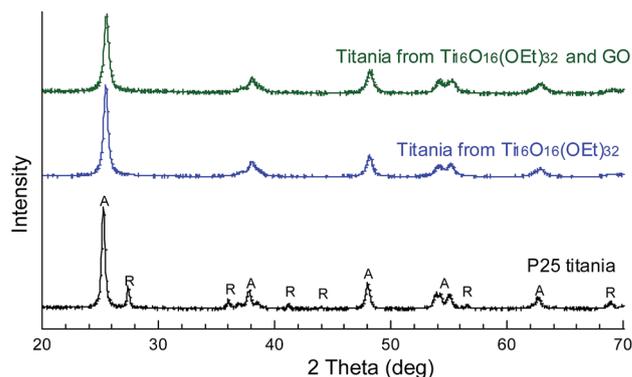

Fig. 4 X-ray diffraction patterns of titania powders prepared by dissolving, drying and calcining $Ti_{16}O_{16}(OEt)_{32}$ clusters, with or without GO, and P25 titania. A: anatase; R: rutile.
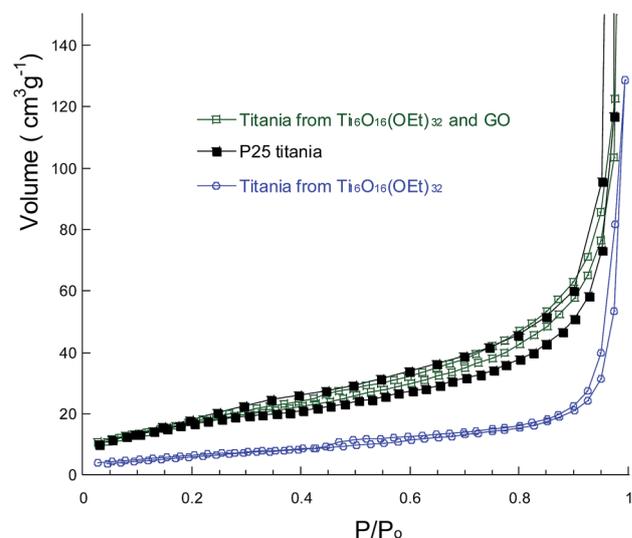

Fig. 5 Nitrogen adsorption isotherms of titania powders prepared by dissolving, drying and calcining $Ti_{16}O_{16}(OEt)_{32}$ clusters, with or without GO, and on P25 titania. Nitrogen adsorption points at 0.994 relative pressure are 534 and 267 cm^3 g^{-1} for P25 and titania from $Ti_{16}O_{16}(OEt)_{32}$ and GO samples. They are omitted in the chart for easier comparison.

reaching 450 °C) result in the sacrifice of the GO, which appears to not be needed in its reduced form to obtain a final titania with enhanced photocatalytic performance. GO's role here is to support or template the formation of nanostructured (<10 nm) particles from $Ti_{16}O_{16}(OEt)_{32}$ decomposition and their arrangement on flakes or layers, which maximises the available surface for light irradiation and photocatalysis. $Ti_{16}O_{16}(OEt)_{32}$ clusters must have anchored on GO flakes by the reaction of hydroxyls on GO basal planes and carboxylic groups on GO edges with the labile terminal ethoxides on the clusters, whose reactivity has been previously demonstrated.[19] Anchoring on GO ensures proper supporting/arrangement of the clusters in two dimensions, leading to a high density of titania nanocrystals arranged on the flakes. The GO therefore avoids dominant arrangement into μm-size globular structures during calcination, where much of the resulting titania would be shielded.

7204 | J. Mater. Chem. A, 2016, 4, 7200–7206

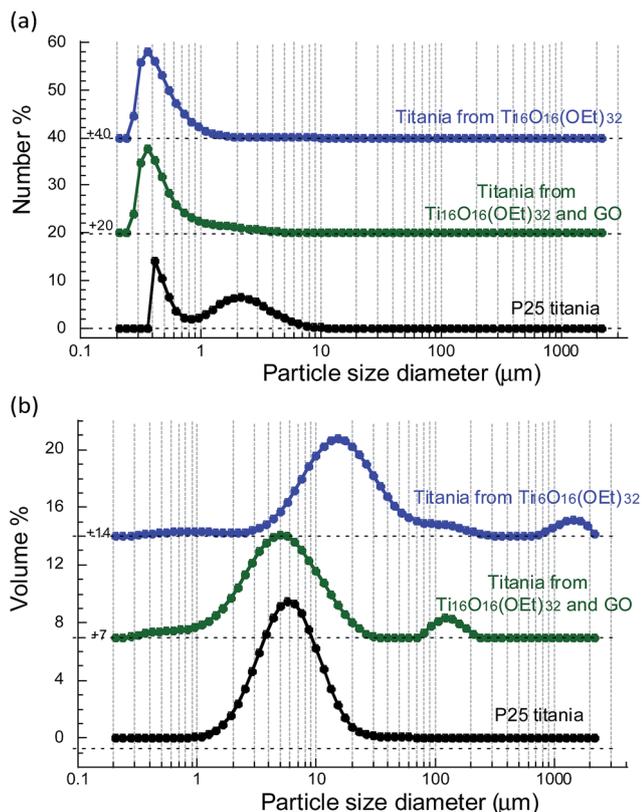This journal is © The Royal Society of Chemistry 2016

Fig. 6 Laser beam scattering (a) number-weighted and (b) volume-weighted equivalent-spherical particle size distribution in suspensions of titania particles prepared by dissolving, drying and calcining $Ti_{16}O_{16}(OEt)_{32}$ clusters, with or without GO. Results for P25 titania are included for comparison. The origin of the y axis of each distribution has been shifted by the indicated values for a clearer comparison.

It is generally believed that P25 titania and other types of rutile-anatase titania provide better photocatalytic performance compared with single-anatase titania due to two factors: (1) the slower recombination resulting from charge stabilisation by electron transfer between phases and (2) the smaller band gap of rutile, which allows more photoexcitation by visible light.[41] However, it is noted here that a pure anatase titania outperforms mixed-phase P25 titania (Fig. 4). This provides evidence that other factors such as morphology, particle size, dispersability and surface area can have a profound effect on the final performance and should also be considered.

These are encouraging results, given that there are many homo- and hetero-metallic oxo alkoxo clusters that remain unused as precursors in photocatalysis, photovoltaics, heterogeneous catalysis and energy applications. The use of GO as a sacrificial support provides a viable and rapid strategy to effectively calcine these precursors and obtain a metal oxide or a mixed metal oxide with nanostructured dimensions and optimised light and reactants' exposure. This opens the door to syntheses of two-dimensional materials with enhanced properties. The many oxygen groups in GO (epoxides, carboxylic groups and hydroxyls) provide anchoring sites for metallic oxo alkoxo clusters, which can facilitate its uniform dispersion/ attachment on two-dimensional flakes and limit grain growth

during calcination. GO is shown here to easily decompose at 450 °C in air within 1 h, likely due to its two-dimensional shape with atomic thickness. Other carbon supports will not imprint the two-dimensional shape, lack anchoring groups and could require higher temperatures and/or longer calcination times for the combustion,[42,43] which could compromise the surface area, particle size and dispersability in water of the metal oxide. We have confirmed that at higher temperatures, such as 550 °C for 1 h, the resulting titania from $Ti_{16}O_{16}(OEt)_{32}$ clusters and GO was aggregated and did not disperse well in water and methanol, therefore, there is an important equilibrium to attain between the sacrifice of the support and the titania formation (i.e., the nucleation and growth of the titania, or in other words, the oxidation of the polyoxotitanium clusters and crystallisation). The use of a cluster with a high degree of condensation (i.e. oxo/Ti ratio, 1 in $Ti_{16}O_{16}(OEt)_{32}$) favours the formation of fine titania particles at low temperature. To confirm this, we followed the same approach to prepare a titania from GO and $Ti(OEt)_4$, where the degree of condensation (oxo/Ti) is 0, and this titania showed much lower photocatalytic performance (7.4 ± 0.7 μmol H_2 g^{-1} h^{-1}). Other clusters with high degree of condensation are $Ti_{17}O_{24}(O^iPr)_{20}$ and $Ti_{18}O_{27}(OH)(O^tBu)_{17}$.[10,44,45] It is also equally important to tailor the chemistry of the cluster and substrate (GO in this case) to promote the anchoring/ support.

Controlling the crystallisation is a critical requirement in many technological applications.[46,47] Inspired by the crystallisation of calcium carbonate structures in organisms, scientists have achieved many breakthroughs using self-assembled monolayers and other organic templates in controlling the location, particle size, shape, crystallographic orientation and composition of crystals.[48,49] It is demonstrated here that GO offers control at two levels. One, GO tunes the nucleation and growth of the nanocrystals resulting from the calcination of $Ti_{16}O_{16}(OEt)_{32}$ clusters, lowering the nanocrystal size down to 8 ± 3 nm. Two, GO shapes the aggregates of these nanocrystals into two-dimensional flakes, an advantageous shape for photocatalysis and other applications.

Conclusion

We have demonstrated a viable and rapid approach to exploit $Ti_{16}O_{16}(OEt)_{32}$ polyoxotitanium clusters in the formation of a titania that outperforms the benchmark P25 titania in photocatalytic hydrogen production by a factor of five. It consists of supporting the clusters on GO before calcination in air and using GO's anchoring sites and two-dimensionality to favour a different nucleation and growth process. This way, titania prepared from $Ti_{16}O_{16}(OEt)_{32}$ clusters ends up having both smaller nanoparticle size (8 vs. 12 nm) and two-dimensionality, replicating GO's flake and layer shape. In addition, or as a consequence, higher surface area, smaller aggregate sizes and better dispersability in aqueous reacting suspensions are obtained. This shows that using GO as a sacrificial support is a viable strategy that can now open the door to the use of many other polyoxometalate clusters for the formation of single or

This journal is © The Royal Society of Chemistry 2016

J. Mater. Chem. A, 2016, 4, 7200–7206 | 7205

mixed metal oxides with unique nanostructure for catalysis, photovoltaics and energy applications.

Acknowledgements

Notes and references

1 S. Styring, *Faraday Discuss.*, 2012, **155**, 357–376.

2 P. C. K. Vesborg and T. F. Jaramillo, *RSC Adv.*, 2012, **2**, 7933–7947.

3 K. Maeda, *J. Photochem. Photobiol., C*, 2011, **12**, 237–268.

4 E. Pastor, F. M. Pesci, A. Reynal, A. D. Handoko, M. J. Guo, X. Q. An, A. J. Cowan, D. R. Klug, J. R. Durrant and J. W. Tang, *Phys. Chem. Chem. Phys.*, 2014, **16**, 5922–5926.

5 S. Navalon, A. Dhakshinamoorthy, M. Alvaro and H. Garcia, *ChemSusChem*, 2013, **6**, 562–577.

6 H. L. Wang, L. S. Zhang, Z. G. Chen, J. Q. Hu, S. J. Li, Z. H. Wang, J. S. Liu and X. C. Wang, *Chem. Soc. Rev.*, 2014, **43**, 5234–5244.

7 H. Tong, S. X. Ouyang, Y. P. Bi, N. Umezawa, M. Oshikiri and J. H. Ye, *Adv. Mater.*, 2012, **24**, 229–251.

8 A. Kudo and Y. Miseki, *Chem. Soc. Rev.*, 2009, **38**, 253–278.

9 T. Hisatomi, J. Kubota and K. Domen, *Chem. Soc. Rev.*, 2014, **43**, 7520–7535.

10 L. Rozes and C. Sanchez, *Chem. Soc. Rev.*, 2011, **40**, 1006–1030.

11 C. Sanchez, L. Rozes, F. Ribot, C. Laberty-Robert, D. Grosso, C. Sassoye, C. Boissiere and L. Nicole, *C. R. Chim.*, 2010, **13**, 3–39.

12 L. Rozes, N. Steunou, G. Fornasieri and C. Sanchez, *Monatsh. Chem.*, 2006, **137**, 501–528.

13 Y. Y. Wu, X. W. Lu, M. Qi, H. C. Su, X. W. Zhao, Q. Y. Zhu and J. Dai, *Inorg. Chem.*, 2014, **53**, 7233–7240.

14 U. Schubert, *Chem. Soc. Rev.*, 2011, **40**, 575–582.

15 P. D. Matthews, T. C. King and D. S. Wright, *Chem. Commun.*, 2014, **50**, 12815–12823.

16 S. Eslava, F. Hengesbach, M. McPartlin and D. S. Wright, *Chem. Commun.*, 2010, **46**, 4701–4703.

17 S. Eslava, B. P. R. Goodwill, M. McPartlin and D. S. Wright, *Inorg. Chem.*, 2011, **50**, 5655–5662.

18 S. Eslava, M. McPartlin, R. I. Thomson, J. M. Rawson and D. S. Wright, *Inorg. Chem.*, 2010, **49**(24), 11532–11540.

19 S. Eslava, A. C. Papageorgiou, S. K. Beaumont, G. Kyriakou, D. S. Wright and R. M. Lambert, *Chem. Mater.*, 2010, **22**, 5174–5178.

20 Y. H. Lai, T. C. King, D. S. Wright and E. Reisner, *Chem.–Eur. J.*, 2013, **19**, 12943–12947.

21 Y. H. Lai, C. Y. Lin, Y. K. Lv, T. C. King, A. Steiner, N. M. Muresan, L. H. Gan, D. S. Wright and E. Reisner, *Chem. Commun.*, 2013, **49**, 4331–4333.

22 G. A. Seisenbaeva and V. G. Kessler, *Nanoscale*, 2014, **6**, 6229–6244.

23 A. Johansson, M. Roman, G. A. Seisenbaeva, L. Kloo, Z. Szabo and V. G. Kessler, *J. Chem. Soc., Dalton Trans.*, 2000, 387–394.

24 V. G. Kessler, *Chem. Commun.*, 2003, 1213–1222.

25 Y. W. Zhu, S. Murali, W. W. Cai, X. S. Li, J. W. Suk, J. R. Potts and R. S. Ruoff, *Adv. Mater.*, 2010, **22**, 3906–3924.

26 W. S. Hummers and R. E. Offeman, *J. Am. Chem. Soc.*, 1958, **80**, 1339.

27 Q. J. Xiang, J. G. Yu and M. Jaroniec, *Chem. Soc. Rev.*, 2012, **41**, 782–796.

28 C. J. Shearer, A. Cherevan and D. Eder, *Adv. Mater.*, 2014, **26**, 2295–2318.

29 K. F. Zhou, Y. H. Zhu, X. L. Yang, X. Jiang and C. Z. Li, *New J. Chem.*, 2011, **35**, 353–359.

30 M. S. A. S. Shah, A. R. Park, K. Zhang, J. H. Park and P. J. Yoo, *ACS Appl. Mater. Interfaces*, 2012, **4**, 3893–3901.

31 A. Mukherji, B. Seger, G. Q. M. Lu and L. Wang, *ACS Nano*, 2011, **5**, 3483–3492.

32 Q. Li, B. Guo, J. Yu, J. Ran, B. Zhang, H. Yan and J. G. Gong, *J. Am. Chem. Soc.*, 2011, **133**, 10878–10884.

33 W. Fan, Q. Lai, Q. Zhang and Y. Wang, *J. Phys. Chem. C*, 2011, **115**, 10694–10701.

34 G. Fornasieri, L. Rozes, S. Le Calve, B. Alonso, D. Massiot, M. N. Rager, M. Evain, K. Boubekeur and C. Sanchez, *J. Am. Chem. Soc.*, 2005, **127**, 4869–4878.

35 M. Hirata, T. Gotou, S. Horiuchi, M. Fujiwara and M. Ohba, *Carbon*, 2004, **42**, 2929–2937.

36 W. Y. Teoh, *Materials*, 2013, **6**, 3194–3212.

37 A. Geim and K. S. Novoselov, *Nat. Mater.*, 2007, **6**, 183–191.

38 K. S. Novoselov, A. K. Geim, S. V. Morozov, D. Jiang, Y. Zhang, S. V. Dubonos, I. V. Grigorieva and A. A. Firsov, *Science*, 2004, **306**, 666–669.

39 B. J. Berne and R. Pecora, *Dynamic Light Scattering: With Applications to Chemistry, Biology, and Physics*, Courier Corporation, 2000.

40 K. Suttiponparnit, J. Jiang, M. Sahu, S. Suvachittanont, T. Charinpanitkul and P. Biswas, *Nanoscale Res. Lett.*, 2011, **6**, 27.

41 D. C. Hurum, A. G. Agrios, K. A. Gray, T. Rajh and M. C. Thurnauer, *J. Phys. Chem. B*, 2003, **107**, 4545–4549.

42 C. J. H. Jacobsen, C. Madsen, T. V. W. Janssens, H. J. Jakobsen and J. Skibsted, *Microporous Mesoporous Mater.*, 2000, **39**, 393–401.

43 K. Zhu, K. Egeblad and C. H. Christensen, *Eur. J. Inorg. Chem.*, 2007, 3955–3960.

44 N. Steunou, G. Kickelbick, K. Boubekeur and C. M. Sanchez, *J. Chem. Soc., Dalton Trans.*, 1999, 3653–3655.

45 C. F. Campana, Y. Chen, V. W. Day, W. G. Klemperer and R. A. Sparks, *J. Chem. Soc., Dalton Trans.*, 1996, 691–702.

46 S. Mann and G. A. Ozin, Synthesis of inorganic materials with complex form, *Nature*, 1996, **382**, 313–318.

47 S. I. Stupp and P. V. Braun, *Science*, 1997, **277**, 1241–1248.

48 F. C. Meldrum and H. Colfen, *Chem. Rev.*, 2008, **108**, 4332–4432.

49 J. Aizenberg, *Adv. Mater.*, 2004, **16**, 1295–1302.